Carcinogenesis vol.13 no.8 pp.1415–1425, 1992

Mutagenesis by (+)-*anti*-B[*a*]P-N^2-Gua, the major adduct of activated benzo[*a*]pyrene, when studied in an *Escherichia coli* plasmid using site-directed methods

William Mackay, Matt Benasutti, Elise Drouin and Edward L.Loechler[1]

Department of Biology, Boston University, Boston, MA 02215, USA

[1]To whom reprint requests should be sent

The suspected major mutagenic adduct of benzo[*a*]pyrene, (+)-*anti*-B[*a*]P-N^2-Gua, is built into the unique *Pst*I recognition site of the *Escherichia coli* plasmid, pUC19, in order to study its mutagenic potential. The adduct can either be at G_{437}, which is replicated during leading strand DNA synthesis, or at G_{438}, which is replicated during lagging strand DNA synthesis. The DNA strand complementary to the strand containing the (+)-*anti*-B[*a*]P-N^2-Gua adduct is saturated with UV lesions to minimize its potential to generate progeny. Although all in-frame mutations could have been detected, a $G_{437} \rightarrow T$ transversion mutation is virtually exclusively obtained at a frequency of ~0.04% per adduct following transformation into Uvr^+ *E.coli* when SOS is not induced, and ~0.18% when SOS is induced. The mutation frequency of the adduct in a Uvr^- background is estimated to be ~0.2% when SOS is not induced, and ~0.9% when SOS is induced. The absence of $G_{438} \rightarrow T$ mutations is rationalized. G → T mutations from (+)-*anti*-B[*a*]P-N^2-Gua are compared to the mutational specificity of the ultimate mutagenic form of activated benzo[*a*]pyrene.

Introduction

Mutagenic processes are fundamental to cancer causation as evidenced by the observation that oncogenes are derived from their normal cellular counterparts (protooncogenes) via mutations (1). Mutagenic events can occur spontaneously or can be induced by exogenous agents (2). Many potent mutagens/carcinogens are bulky and three-dimensionally complex, such as benzo[*a*]pyrene (B[*a*]P*), aflatoxin B_1 (AFB_1), 2-aminofluorene (2-AF), 2-acetylaminofluorene (2-AAF) and *cis*-diammindichloroplatinum(II) (*cis*-DDP), and understanding the mechanisms by which they induce mutations is only now becoming possible (3–7).

B[*a*]P, a polycyclic aromatic hydrocarbon, reacts with DNA following activation to its corresponding 7,8-diol-9,10-epoxide (BPDE) (reviewed in refs 8 and 9). The majority of adducts *in vivo* are thought to be derived from the (+)-*anti*-isomer of BPDE (Figure 1) (8,9), though this may not always be the case (10–12). The most prevalent adducts derived from the racemic mixture of (±)-*anti*-BPDE are B[*a*]P-N^2-Gua (Figure 1) (8,9,13–15) and B[*a*]P-N^6-Ade (16), where *trans* addition to the epoxide prevails, as well as B[*a*]P-*N*(7)-Gua (17,18), which has not been carefully characterized. In addition, evidence exists for the formation of cytosine adducts (19,20).

The adducts of (±)-*anti*-BPDE are reported to block DNA replication (21), and induce homologous (22) and illegitimate recombination (23). In addition (±)-*anti*-BPDE is mutagenic and induces both base pairing and insertion/deletion mutations (24–35). The mutational specificity of the racemic mixture of (±)-*anti*-BPDE in bacteria has been determined in several systems; the most prevalent mutations are GC → TA and AT → TA (27–29). Mutational spectra for (±)-*anti*-BPDE have been determined in human cells using a shuttle vector system, (30), and in CHO cells (31,32) and human cells (33–35) using endogenous target genes, where the specificity is reasonably similar to that determined in bacteria, though GC → CG mutations appear to become more prevalent. Mutations induced in the Ha-*ras* oncogene at the 61st codon have been determined with cells in culture (36). Finally, GC → TA and AT → TA mutations in Ha-*ras* have been identified in tumors derived from animals treated with B[*a*]P (1, 37–39).

Although much information is known about both the adducts and the mutations arising from BPDE, the relationship between these two is poorly understood. During the last several years it has become possible to study the biological consequences of individual DNA adducts because of the development of techniques

***Abbreviations:** B[*a*]P, benzo[*a*]pyrene; (+)-*anti*-BPDE, (+)-*r*-7,*t*-8-dihydroxy-*t*-9,10-epoxy-7,8,9,10-tetrahydrobenzo[*a*]pyrene (*anti*) (Figure 1); (+)-*anti*-B[*a*]P-N^2-Gua, the *trans* additional product between the *C*10 position of (+)-*anti*-BPDE and the N^2 position of guanine (Figure 1); *cis*-DDP(GpG), the *N*(7)Gua-*N*(7)-Gua diadduct of *cis*-diammindichloroplatinum(II); *cis*-DDP(ApG), the *N*(7)Ade-*N*(7)-Gua diadduct of *cis*-DDP; AF-C8-Gua, the *C*(8)-Gua adduct of 2-aminofluorene; AAF-C8-Gua, the *C*(8)-Gua adduct of 2-acetylaminofluorene; AFB_1-N7-Gua, the *N*(7)-Gua adduct of aflatoxin B_1; 5′-pT(B[*a*]P-N^2)GCA-3′, an oligonucleotide containing (+)-*anti*-B[*a*]P-N^2-Gua; (+)-*anti*-B[*a*]P-N^2-Gua-pUC19, the plasmid pUC19 with 5′-pT(B[*a*]P-N^2)GCA-3′ ligated into the *Pst*I recognition site; C-pUC19, the plasmid pUC19 with 5′-TGCA-3′ ligated into the *Pst*I recognition site; IPTG, isopropyl β-D-thiogalactopyranoside; X-gal, 5-bromo-4-chloro-3-indoyl β-D-galactopyranoside; WT^b, $PstI^+$ (blue); M^b, $PstI^-$ (blue); M^w, $PstI^-$ (white); M^{lb}, $PstI^-$ (light blue); M^{fb}, $PstI^-$ (faintly blue)—the latter five abbreviations are presented more thoroughly in Table II; R_i is defined in equation (1) (Materials and methods); $R_{G\rightarrow T}$ is defined in equation (2a) (Materials and methods); $MF_{G\rightarrow T}^{+ER}$ is defined in equations (3) and (4) (Materials and methods) and $MF_{G\rightarrow T}^{-ER}$ is defined in equation (5) (Materials and methods); *MF*, mutation frequency; +ER, excision repair proficient cells (AB1157); −ER, excision repair deficient cells (AB1885); ds, double strand.

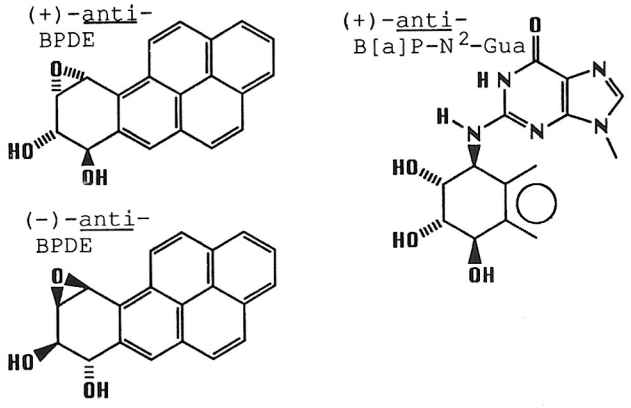

Fig. 1. Structures of (+)-*anti*-BPDE, (−)-*anti*-BPDE, and the adduct, (+)-*anti*-B[*a*]P-N^2-Gua (*trans* addition).

to construct DNA vectors that contain adducts of defined chemical structure at known genome locations (reviewed in 3; 4–7,40).

Considerable attention has been focused upon the major adduct of BPDE, formed at N^2-Gua, in relationship to carcinogenesis, with the implicit assumption that this adduct is capable of inducing mutations *in vivo*. In an effort to begin to evaluate this crucial assumption we have undertaken site-directed studies (Figure 2; 40) on the mutations induced by (+)-*anti*-B[*a*]P-N^2-Gua. We show that a targeted G → T mutation predominated in *Escherichia coli* and is enhanced ~4-fold following SOS induction.

These results are discussed in the light of the mutational specificity of BPDE. The most striking comparison is that in random mutagenesis studies with (+)-*anti*-BPDE only GC → TA mutations are obtained in 5′-TG-3′ sequence contexts. The results reported herein are for a (+)-*anti*-B[*a*]P-N^2-Gua adduct in a 5′-TG-3′ sequence context, which also gave only G → T mutations. This suggests that (+)-*anti*-B[*a*]P-N^2-Gua could be principally responsible for the mutations from (+)-*anti*-BPDE, at least in the sequence context used in this study.

Materials and methods

(+)-*anti*-BPDE was handled as described previously (40). All materials, including the synthesis of 5′-pT[B[*a*]P-N^2]GCA-3′, which is the oligonucleotide containing (+)-*anti*-B[*a*]P-N^2-Gua, as well as the basic procedures (Figure 2) have been described previously (40). All restriction digests were performed in the manufacturer's recommended buffers (40), and all units are as defined by the manufacturer (40).

Bacterial strains

AB1157 and AB1885 cells (*uvrB5*) (41) were obtained from Dr G.Walker, Massachusetts Institutes of Technology. NR8044 is an opal suppressor, *lacZΔM15* strain that was obtained from Dr J.Essigmann, Massachusetts Institutes of Technology. DH5-α cells (42) were obtained from Dr D.Tolan, Boston University.

Gapped duplex construction

pUC19 (500 μg) was treated with *Pst*I (1200 units) to give linear DNA with a four base, 3′-overhanging end of sequence, 5′-TGCA-3′ (Figure 2; step 1). These four bases were removed in a blunt-ending reaction by incubation with 34 units of T4 DNA polymerase for 30 min (Figure 2; step 2) to remove ~70 bases (as estimated by methods described previously; see ref. 40) from both 3′-ends (10 mM Tris–HCl/1 mM EDTA/10 mM $MgCl_2$, pH 8.0; 5 ml) After 30 min, an additional 34 units were added with dATP, dCTP, dGTP and dTTP (120 μM each). DNA synthesis proceeded for 30 min (37°C) after which the solution was made 9 mM EDTA (pH 8.0), cooled on ice and precipitated with ethanol.

pUC19 (500 μg) was cleaved with *Sca*I (step 3 in Figure 2; New England Biolabs; 3000 units) and irradiated with UV light (step 4 in Figure 2; 4800 J/m^2 in 10 mM Tris–HCl/1 mM EDTA, pH 8.0). pUC19, itself, when irradiated in parallel and transformed into AB1157 cells, gave a surviving fraction of $<10^{-6}$. This represents a saturating dose of UV light, and we estimate that >14 pyrimidine dimers and 5 [6–4] lesions were induced per strand (43). UV-irradiated pUC19 was stored for 6 months and shown to continue to have a surviving fraction of $<10^{-6}$, which demonstrated that, upon prolonged storage, the UV lesions do not become converted into adducts that are less lethal.

*Sca*I- and *Pst*I-digested DNA (225 μg of each) were mixed (188 mM KCl/13 mM Tris–HCl, pH 7.5; 10 ml) and denatured/renatured (Figure 2; step 5) to give gapped duplexes as described previously (40). In fact four species are generated as indicated in Figure 2. (We note that plasmids are represented both as ovals and circles in Figure 2 for convenience; and that, for example, step 6A implies step 6 in pathway A.) There are two gapped duplexes missing the bases, 5′-TGCA-3′ in either the (+) strand (pathway A in Figure 2) or the (−) strand (pathway B in Figure 2), as well as starting material, which includes linear *Pst*I-cleaved plasmids that were blunt ended (pathway C in Figure 2) and linear *Sca*I-cleaved plasmids that have UV lesions (pathway D in Figure 2). Each of these four species represented ~25% of the mixture. This mixture was purified by CsCl density gradient centrifugation, ethanol precipitated and resuspended in 10 mM Tris–HCl/1 mM EDTA/50% glycerol (pH 8.0) and stored at −20°C.

Construction of (+)-anti-B[a]P-N^2-Gua-pUC19

Approximately 2.9 μg of gapped duplexes (which also contained ~2.9 μg of linear DNA) was mixed with 0.56 μg (473 pmol) of purified 5′-pT(B[*a*]P-N^2)GCA-3′ (an ~250-fold molar excess) in the presence of 1.5 mM ATP; T4 DNA ligase (2000 units) was added and incubated at 17°C (step 6 in Figure 2). At 7 and

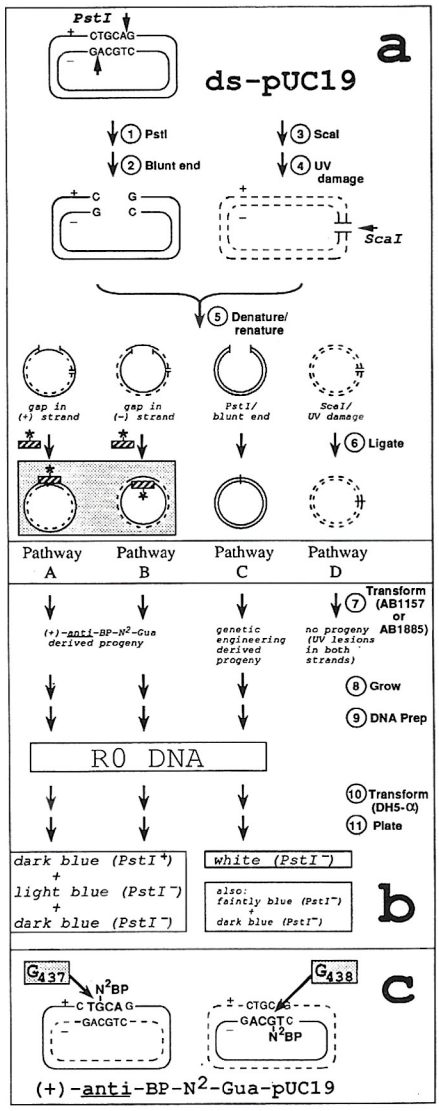

Fig. 2. Strategy for situating (+)-*anti*-B[*a*]P-N^2-Gua in the *Pst*I recognition site of pUC19 to give (+)-*anti*-B[*a*]P-N^2-Gua-pUC19 (**panel a**), which is an equal mixture containing an adduct either at G_{437} or G_{438} (**panel c**), and the mutant enrichment strategy (**panel b**). (**a**) Denaturation/renaturation (step 5) led to the formation of a (+)-strand gapped duplex and a (−)-strand gapped duplex, as well as linear DNA, where the latter is merely the starting material for step 5, which is either linear *Pst*I/blunt or *Sca*I/UV. *Sca*I-cleaved pUC19 is indicated by dashed lines to show that it was UV irradiated and was less viable as a result. The large shaded box shows (+)-*anti*-B[*a*]P-N^2-Gua-pUC19, which was formed by the ligation (step 6) of the oligonucleotide 5′-T[B[*a*]P-N^2]GCA-3′ (cross-hatched box with an asterisk), into a gapped duplex in either the plus or minus strands. Plus and minus signs indicate the strand being copied during leading and lagging strand DNA replication respectively. Linear pUC19 that was cleaved with *Pst*I and blunt-ended can blunt-end ligate to form circular DNA missing four bases at the *Pst*I recognition site. Linear pUC19 that was cleaved with *Sca*I and UV-irradiated also could blunt-end ligate to form circular DNA. (**b**) Following steps 7–9 (Materials and methods), plasmid DNA (designated R0) was obtained, which is a mixture derived from pathways A–C. Pathway D gives virtually no progeny because both DNA strands contain UV damage. Following steps 10 and 11, R0 DNA: (i) from pathways A and B generated colonies that appeared either dark blue (both *Pst*$^+$ and *Pst*$^-$) or light blue (*Pst*I$^-$); and (ii) from pathway C generated colonies that appeared white (*Pst*$^-$). In steps analogous to pathway C, progeny plasmids that appeared faintly blue or dark blue (both *Pst*I$^-$) could also be generated; these are due to 5 bp deletions and 6 bp deletions respectively in the *Pst*I site (Materials and methods). (**c**) Ligation of 5′-pT[B[*a*]P-N^2]GCA-3′ into the (+)-strand results in the adducts being at position G_{437}. Ligation of 5′-pT[B[*a*]P-N^2]GCA-3′ into the (−)-strand results in the adducts being at position G_{438}.

18 h, equivalent amounts of ligase and ATP were added again (final volume 344 μl). The reaction was stopped after a total of 24 h. The mixture was drop dialyzed (40) against 10 mM Tris−HCl/1 mM EDTA (pH 8.0) for 2 h and the products purified by gel exclusion chromatography (Sepharose CL-4B). The material in the void volume was stored in 10 mM Tris−HCl/1 mM EDTA/20% glycerol (pH 8.0) and is designated (+)-*anti*-B[*a*]P-N^2-Gua-pUC19.

To ensure that any gapped duplexes remaining after ligation did not give rise to wild-type progeny during transformation, the (+)-*anti*-B[*a*]P-N^2-Gua-pUC19 ligation mixture was incubated with DNA polymerase I Klenow fragment and dATP, dCTP, dGTP and dTTP. Gapped duplexes filled in by this procedure are cleavable by *Pst*I, which reduces their transformation efficiency by >98% (data not shown). Following *Pst*I digestion, the DNA was purified with an ELUTIP according to the manufacturer's (Schleicher and Schuell) procedure. The material was ethanol precipitated and resuspended in 10 mM Tris−HCl/1 mM EDTA/50% glycerol (pH 8.0; 20 μl) and stored at −20°C. The final yield of (+)-*anti*-B[*a*]P-N^2-Gua-pUC19 was estimated as described previously (40) to be ~16% and was ~6-fold lower than the yield for C-pUC19 (98%), which is a control plasmid constructed similarly by the ligation of the unadducted oligonucleotide, 5′-TGCA-3′, into the same gapped duplex.

Transformations of (+)-anti-B[a]P-N^2-Gua-pUC19 into E.coli

Transformation was conducted by electroporation (44). When SOS induction was studied, it was accomplished by the method of Fuchs (45); either AB1157 or AB1885 cells were suspended in 10 mM $MgSO_4$ (following harvesting) and irradiated with UV light (Ultraviolet Products, Inc., Model UAG-54) at 24 or 1.5 J/m^2 respectively, which gave a cell survival fraction of 40 or 22% respectively. Thereafter, the cells were pelleted and resuspended in ice-cold distilled water twice according to the protocol for transformation by electroporation (44); the procedure took ~90 min. Competent cells (40 μl) were mixed with plasmid DNA, of which ~5 ng was adduct containing (+)-*anti*-B[*a*]P-N^2-Gua-pUC19, and transformed by electroporation (BioRad Gene Pulsar; 2500 V, 100 ohms, 25 μF using a 0.2 cm gapped cuvette) as indicated in step 7 of Figure 2.

It is unlikely that electroporation affects the adduct. In a separate experiment, 5′-pT[B[*a*]P-N^2]GCA-3′ was subjected to electroporation using conditions identical to those cited above. There was no evidence for degradation of the oligonucleotide when analyzed by methods described previously (40). For example, 5′-pT[B[*a*]P-N^2]GCA-3′ gave no discernible breakdown products at the level of ~1% as assessed by the appearance of unexpected ^{32}P-containing bands following polyacrylamide gel electrophoresis or ^{32}P-containing peaks following HPLC analysis.

Following a 2 h recovery (37°C in 1 ml of LB) after electroporation, a fraction of the transformation mixture was plated to determine the total number of transformants; ~2.5 × 10^6 and ~10 × 10^6 colonies were obtained from (+)-*anti*-B[*a*]P-N^2-Gua and C-pUC19 respectively; SOS induction did not significantly alter the yield (see Results). (It was impossible at this stage to obtain information about the relative numbers of colonies that appeared blue, white, etc., because AB1157 and AB1885 cells are not designed for α-complementation.) LB (20 ml; 100 μg/ml ampicillin) was added to the remainder of the cells, which were grown overnight (Figure 2; step 8). One ml of this mixture was added to 40 ml of LB (100 μg/ml ampicillin) and grown overnight. Plasmid DNA (~100 μg) was isolated from these cells and was purified by CsCl density gradient centrifugation (Figure 2; step 9). It is designated R0 DNA, to indicate that it has not been subjected to mutant enrichment (see below). R0 DNA was transformed by electroporation into DH5-α cells and plated (Figure 2; steps 10 and 11). Greater than 95% of the colonies appeared either blue or white at this stage, though ultimately light blue and faintly blue colonies were also definitively identified (see below). The ratio of blue to white colonies was determined for each sample (R_i, where 'i' indicates initial; Table I), and light blue and faintly blue colonies were scored as white, initially.

Mutant enrichment procedure

Progeny plasmids from the adduct in (+)-*anti*-B[*a*]P-N^2-Gua-pUC19 ligations (i.e. following pathways A and B in Figure 2) gave a mixture of blue and light blue colonies following step 11 in Figure 2. The majority of the blue colonies from all of the transformations was *Pst*I$^+$ wild-type. (We note that the designation *Pst*I^s is more correct than *Pst*I$^+$, but the latter is easier to understand in the context of this study.) *Pst*I treatment of R0 DNA gave DNA designated R1 (Figure 3; step 1), which when retransformed and plated (Figure 3; step 2) preferentially gave colonies from mutant (*Pst*I$^-$) DNA, because *Pst*I$^+$ DNA was linearized, which decreased its transformation efficiency. (We note that on some occasions R1 DNA was transformed into cells that were grown overnight and plasmid DNA was isolated from these cells; this is also designated R1 DNA, but could be stored as a permanent stock.) One round of *Pst*I enrichment was sufficient to remove wild-type DNA from transformations with (+)-*anti*-B[*a*]P-N^2-Gua-pUC19, while two rounds of enrichment were required for C-pUC19. We note that if, prior to transformation, linearized (i.e. *Pst*I-cleaved) plasmids were heated for 5 min at 65°C and placed on ice, then the yield of transformants was decreased significantly. Thus, this step was included in all cases.

In addition to mutants derived from the adduct in (+)-*anti*-B[*a*]P-N^2-Gua-pUC19, several mutations were isolated that can be attributed to side-reactions in the genetic engineering protocol. These gave rise to white, faintly blue and dark blue colonies as indicated after step 11C in Figure 2(b). All of these mutations are discussed below, beginning with those derived from genetic engineering side-reactions. A key to the relationship between colony color and the nature of the plasmid in the colony is given in Table II. Table II also lists an estimate of the approximate percentage that each plasmid contributed to the original transformation of (+)-*anti*-B[*a*]P-N^2-Gua-pUC19 into SOS induced AB1157 cells.

White mutants

During the ligation of 5′-pT(B[*a*]P-N^2)GCA-3′ into the gapped duplexes (i.e. steps 6A and 6B in Figure 2), a competing reaction occurred (46−48). Following denaturation/renaturation (step 5 in Figure 2), ~50% of the DNA gave gapped duplexes, which is represented as the two species above pathways A and B in Figure 2. However, ~50% of the DNA re-forms linear molecules, which is

Table I. Analysis of progeny plasmids derived from (+)-*anti*-B[*a*]P-N^2-Gua-pUC19 and C-pUC19 in *Escherichia coli*

	Results in AB1157 cells (*uvr*$^+$)			Results in AB1885 cells (*uvrB5*)		
	R_i(AB1157)[a]	$R_{G\to T}$[b]	$MF_{G\to T}^{+ER}$[c]	R_i(AB1886)[a]	$\frac{[R_i(AB1157)]}{[R_i(AB1886)]}$[d]	$MF_{G\to T}^{-ER}$[e]
(+)-anti-B[a]P-N^2-Gua-pUC19						
+SOS[f]	0.087	57/358 000	0.18×10^{-2}	0.018	4.9	0.87×10^{-2}
−SOS	0.093	15/369 000	0.044×10^{-2}	0.017	5.4	0.24×10^{-2}
C-pUC19						
+SOS[f]	0.69	0/491 000	$<0.30 \times 10^{-5}$	0.44	1.5	$<0.45 \times 10^{-5}$
−SOS	0.71	2/848 000	0.33×10^{-5}	0.37	1.7	0.55×10^{-5}

[a] $R_i = [WT^b + M^b]/[M^w + M^{lb} + M^{fb}]$ is equation (1) (Materials and methods), where the symbols are found in Table II. Importantly, M^{lb} indicates plasmids with $G_{437} \to T$ mutations. R_i(AB1157) was determined in AB1157 cells, while R_i(AB1885) was determined in AB1885 cells. R_i is the average of four determinations.

[b] $R_{G\to T} = [M^{lb}]/[M^w + M^{lb} + M^{fb}]$ is equation (2b) (Materials and methods), and is the ratio of $G_{437} \to T$ mutations (i.e. M^{lb}) to total plasmids following the mutant enrichment procedure that eliminated wild-type, *Pst*I$^+$ plasmids (i.e. WT^b). $G_{437} \to T$ mutations were determined by methods 1 and 2 (Figure 3), while the denominator was estimated by counting representative plates.

[c] $MF_{G\to T}^{+ER}$ is the mutation frequency for $G_{437} \to T$ mutations in excision repair proficient cells (i.e. AB1157) and can be calculated from the ratios R_i and $R_{G\to T}$ according to equation (4) (Materials and methods).

[d] This value is merely the ratio R_i(AB1157)/R_i(AB1885), where the values for R_i(AB1157) and R_i(AB1885) come from the first and fourth columns respectively.

[e] $MF_{G\to T}^{-ER}$, which is the mutation frequency for $G_{437} \to T$ mutations in excision repair deficient (i.e. AB1885) cells, is calculated according to equation (5) (Materials and methods).

[f] SOS induction is described in Materials and methods.

represented as the top drawings in pathways C and D in Figure 2, and which can blunt-end ligate. During ligation, the *Pst*I cleaved/blunt-end, linear DNA circularizes (Figure 2; step 6C) and upon transformation (Figure 2; step 7C) generated progeny that were missing $\overset{5'\text{-}TGCA\text{-}3'}{5'\text{-}ACGT\text{-}5'}$ from the *Pst*I site and thus were both *Pst*I insensitive and ultimately gave white colonies because of the 4 bp

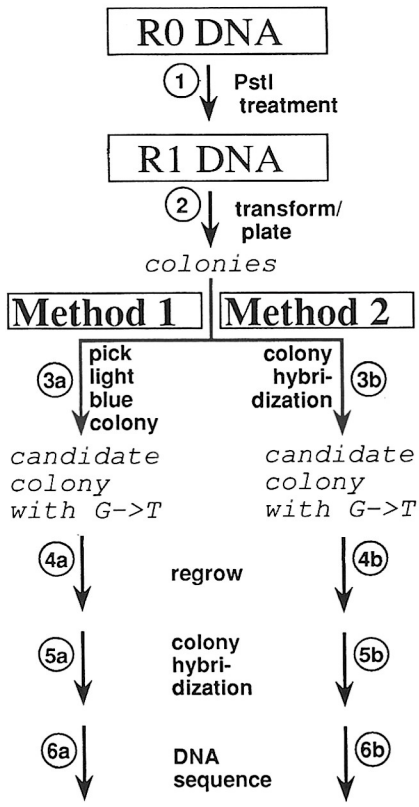

Fig. 3. Mutant isolation procedure. R0 DNA, which is a mixture of species (see step 9 in Figure 2), was treated with *Pst*I. *Pst*I$^+$ wild-type plasmids in the mixture were linearized by *Pst*I treatment (step 1), while *Pst*I$^-$ mutant plasmids remain closed circular; this mixture is designated R1 DNA. Linearized plasmids do not transform efficiently, so after step 2 colonies are enriched for plasmids that contain *Pst*I$^-$ material. Two methods were used to isolate a $G_{437} \rightarrow T$ mutation. Colonies containing this mutant plasmid were detectable by a phenotypic screen (see Results), because they appeared light blue in an opal suppressor strain. **Method 1:** all light blue (as well as faintly blue colonies) were picked (step 3a), regrown (step 4a) and subjected to colony hybridization with an oligonucleotide complementary to the $G_{437} \rightarrow T$ mutation (step 5a). Positive colonies were confirmed by DNA sequencing (step 6a). **Method 2:** the same plates used in method 1 (i.e. after step 2 in Figure 3) were also subjected to colony hybridization using the $G_{437} \rightarrow T$ specific oligonucleotide probe (step 3b). Plugs of agar were collected from the regions of the plates where positive signals were detected. Colonies were grown on plates (step 4b) from these plugs and screened using the same probe (step 5b). Positive colonies were confirmed by DNA sequencing (step 6b).

frameshift mutation in the *lacZ'* fragment of pUC19 (i.e. after step 11C in Figure 2). Numerous white mutants were shown to be 4 bp deletion mutations by DNA sequencing during the course of this study. This kind of side-reaction has been noted in a number of site-directed mutagenesis studies (46–48). During ligation, the *Sca*I-cleaved/UV-irradiated, linear DNA also circularizes (Figure 2; step 6D), but upon transformation (Figure 2; step 7D) generates virtually no progeny because both DNA strands contained UV damage, which was established to reduce viability by $>10^6$-fold.

Faintly blue mutants. Five-base deletion mutants with end-points at the *Pst*I cleavage site were also detected at a frequency of ~5%. Mutants of this type were recently detected in a similar site-directed study involving a *cis*-DDP adduct with an M13mp19 vector (L.N.Naser-Bradley and J.M.Essigmann, personal communication). If some of the molecules in the blunt-ending reaction (Figure 2; step 2) had an additional base removed from their 3′ end via nibbling with T4 DNA polymerase, then ligation (step 6C in Figure 2) would recircularize these molecules to give material missing 5 bp in the *Pst*I recognition site. One 5 base deletion was missing bases 435–439 in the *Pst*I recognition site, while a second was missing bases 436–440 in the *Pst*I recognition site. The former was generated ~12 times more frequently than the latter as shown by DNA sequencing.

In principle, 5 bp deletion mutants should ultimately generate white colonies (i.e. after step 11C in Figure 2) because their reading frame is −2; in fact, they appear faintly blue. Based upon the sequence of pUC19, the first stop codon encountered in the 5 bp deletion mutants is opal and is located upstream of the important coding region in *lacZ'*. This result forced us to conclude that opal stop codons permit ribosomes to re-engage mRNA after termination and do so in-frame. Such effects have been reported and this and other unusual effects in translation are often associated with opal stop codons (49,50).

Dark blue mutants. Following mutant enrichment by *Pst*I digestion of R0 DNA from transformations with both (+)-*anti*-B[*a*]P-N^2-Gua-pUC19 and C-pUC19 (Figure 3; step 1), dark blue mutants were obtained (Figure 3; step 2). Genetic engineering-derived, 6 bp deletion mutants with end-points at the *Pst*I cleavage site were occasionally identified; 15 were obtained during the course of all of the work described herein. These are in-frame deletions that result in dark blue colonies. We attribute the formation of these mutants to the same mechanism that led to the formation of the faintly blue, 5 base deletion mutants via pathway C in Figure 2.

Following mutant enrichment by *Pst*I digestion of R0 DNA from transformations with (+)-*anti*-B[*a*]P-N^2-Gua-pUC19 (i.e. after step 2 in Figure 3), one dark blue mutant not attributable to genetic engineering side reactions was isolated and sequenced; it was a $G_{437} \rightarrow C$ mutation.

Light blue mutants. A $G_{437} \rightarrow T$ mutation during leading strand replication of (+)-*anti*-B[*a*]P-N^2-Gua generates an opal stop codon in the *lacZ'* fragment, which is pathway A in Figure 2. Colonies containing this mutant plasmid were detectable by a phenotypic screen, i.e. they appeared light blue in the opal suppressor strain, NR8044 (Figure 2; step 11A). Two methods were used to isolate $G_{437} \rightarrow T$ mutations and both began with transformation and plating of R1 DNA (Figure 3; step 2). ($G_{437} \rightarrow T$ mutations also appeared light blue in non-opal suppressor strains, but were darker in hue than the 5 bp deletion mutants in the opal suppressor strain, presumably because suppression augments ribosome restart.)

Method 1. All light blue (as well as faintly blue) colonies were picked (Figure 3; step 3a). These colonies were regrown (Figure 3; step 4a) and subjected to colony hybridization (51) with the oligonucleotide 5′-TCGACCTTCAGGCATG-3′, which is complementary to the $G_{437} \rightarrow T$ mutation (Figure 3; step 5a). Figure 4(a) shows an example of colony hybridization. Colonies were confirmed by double-stranded (ds) DNA sequencing (Figure 3; step 6a) using the dideoxynucleotide method (ref. 52 with slight modification).

Method 2. To guarantee that no $G_{437} \rightarrow T$ transversion mutations were missed using method 1, colony hybridization was conducted directly on the same plates from which the light blue mutants were picked in method 1. Light blue colonies

Table II. Key to the nature of the observed mutations when (+)-*anti*-B[*a*]P-N^2-Gua-pUC19 was transformed into SOS-induced AB1157 cells

B[*a*]P adduct pathways					Genetic engineering pathways				
Colony color	*Pst*I sequence	Symbol	~% of trans.[a]	Source	Colony color	*Pst*I sequence	Symbol	~% of trans.[a]	Source
1. dark blue	wild-type	WT^b	8	no mutation	1. white	mutant	M^w	87	4 base deletion
2. light blue	mutant	M^{lb}	0.2	$G_{437} \rightarrow T$	2. faintly blue	mutant	M^{fb}	5	5 base deletion
3. dark blue	mutant	M^b	<0.01	$G_{437} \rightarrow C$	3. dark blue	mutant	M^b	~0.02	6 base deletion

[a]Estimated percentage of transformants after step 6 in Figure 3 based upon all of the results. WT^b is from R_i in Table I. M^{lb} is estimated based upon $MF_{G\rightarrow T}^{+ER}$ in Table I. M^b is estimated from that fact that only one $G_{437} \rightarrow C$ mutation was detected compared to 57 $G_{437} \rightarrow T$ mutations (Table I). M^w is from R_i in Table I. M^{fb} is from the fact that ~24/25 of the (light blue + faintly blue) colonies picked in step 3a in Figure 4 proved to be faintly blue and not light blue. M^b is estimated based on the fact that only four of these mutants were obtained throughout the work with (+)-*anti*-B[*a*]P-N^2-Gua-pUC19 transformed into SOS-induced AB1157 cells.

were picked, but not obliterated, and method 1 followed (i.e. steps 3–6A in Figure 3). Subsequently, the same plates from step 2 in Figure 3 were also subjected to colony hybridization using the $G_{437} \rightarrow T$ specific oligonucleotide probe (Figure 3; step 3b). An example of a colony hybridization involving an entire plate is shown in Figure 4(b). Plugs of agar were collected from the regions of the plates where positive signals were detected. Colonies were grown from these plugs (Figure 3; step 4b) and rescreened using the $G_{437} \rightarrow T$ oligonucleotide probe (Figure 3; step 5b). Positive colonies were corroborated by DNA sequencing (Figure 3; step 6b).

Mutants were collected 3, 2, 2 and 1 times with (+)-*anti*-B[*a*]P-N^2-Gua-pUC19 (+SOS), (+)-*anti*-B[*a*]P-N^2-Gua-pUC19 (−SOS), C-pUC19 (+SOS) and C-pUC19 (−SOS) respectively. In one instance with (+)-*anti*-B[*a*]P-N^2-Gua-pUC19 (+SOS), 23 mutants were isolated by method 1, and no mutants were uniquely identified by method 2, while in another instance with (+)-*anti*-BP-N^2-Gua-pUC19 in SOS-induced cells, 23 mutants were isolated by method 1, and three mutants were uniquely identified by method 2. These results suggested that method 1 alone was reasonably reliable, and it was used alone in one case each with (+)-*anti*-B[*a*]P-N^2-Gua-pUC19 (+SOS), (+)-*anti*-B[*a*]P-N^2-Gua-pUC19 (−SOS) and C-pUC19 (+SOS), but not with C-pUC19 (−SOS).

Mutation frequency calculation

The only mutation that occurred at a reasonably high frequency was a $G_{437} \rightarrow T$ mutation, and the method to calculate its mutation frequency is described. We use the results from the transformations with (+)-*anti*-B[*a*]P-N^2-Gua-pUC19 into SOS induced, AB1157 cells as an example, but essentially all of the calculations are similar.

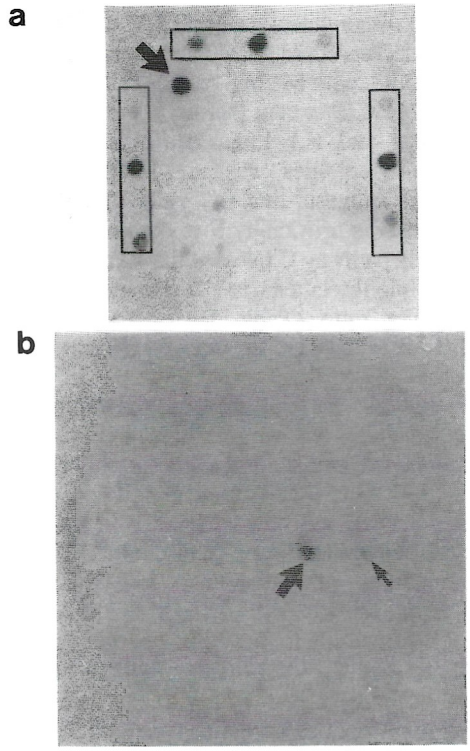

Fig. 4. Oligonucleotide (5′-[^{32}P]-TCGACTTCAGGCATG-3′) blotting of colonies to isolate $G_{437} \rightarrow T$ mutations. (**a**) The top panel shows colony hybridization after step 5a in Figure 3 (method 1). Light blue and faintly blue colonies were isolated from plates (Figure 3; step 3a) and regrown (Figure 3; step 4a), transferred to nitrocellulose filters and blotted (Figure 3; step 5a). Standards are shown in the three boxes: in all cases the strongest signal is $G_{437} \rightarrow T$ mutation; the intermediate signal is wild-type (i.e. *Pst*I$^+$); and the weakest signal is the 5 bp deletion mutation. One positive colony (out of 25) is apparent and is indicated by the arrow. (**b**) The bottom panel shows colony hybridization after step 3b in Figure 3 (method 2). Approximately 2000 colonies on a plate were transferred to a nitrocellulose filter and blotted with the oligonucleotide probe that was specific for the $G_{437} \rightarrow T$ mutation (Figure 3; step 3b). Two colonies appeared positive; plugs were removed from the original plate, grown (Figure 3; step 4b) and subjected to colony hybridization (Figure 3; step 5b). A representative positive colony was picked and its plasmid DNA isolated for DNA sequencing (Figure 3; step 6b). One of the original colonies proved to be a $G_{437} \rightarrow T$ mutant (larger arrow), while the other was a false positive (smaller arrow).

The ratio of blue to 'white' colonies, R_i(AB1157) = 0.087 (Table I), was ascertained following step 11 in Figure 2 and is the average of four determinations. R_i(AB1157) can be expressed mathematically as

$$R_i(\text{AB1157}) = (\text{blue})/(\text{white} + \text{light blue} + \text{faintly blue}) = [WT^b + M^b]/[M^w + M^{lb} + M^{fb}] \quad (1)$$

where WT^b represents blue (*Pst*I$^+$) colonies, M^b represents blue (*Pst*I$^-$) colonies, M^w represents white (*Pst*I$^-$) colonies; M^{lb} represents light blue (*Pst*I$^-$) colonies, which have a $G_{437} \rightarrow T$ mutation; and M^{fb} represents faintly blue (*Pst*I$^-$) colonies (Table II). We note that light blue and faintly blue mutants appeared closer to white than blue in color and thus were included in the denominator of equation (1).

$R_{G\rightarrow T}$ represents the ratio of $G_{437} \rightarrow T$ mutations (i.e. M^{lb}) to total mutations following the mutant enrichment procedure (Figure 3) that eliminated wild-type, *Pst*I$^+$ plasmids (i.e. WT^b), and can be expressed as

$$R_{G\rightarrow T} = [M^{lb}]/[M^w + M^{lb} + M^{fb} + M^b] \quad (2a)$$

From Table II, $(M^w + M^{lb} + M^{fb}) \gg (M^b)$, then

$$R_{G\rightarrow T} \simeq [M^{lb}]/[M^w + M^{lb} + M^{fb}] \quad (2b)$$

A total of 358 000 colonies, which was determined by counting representative plates, were screened by methods 1 and 2 (see above) and 57 $G_{437} \rightarrow T$ mutations were isolated (Table I).

$MF_{G\rightarrow T}^{+ER}$ is the mutant frequency for $G_{437} \rightarrow T$ mutations in excision repair proficient cells (i.e. AB1157) and can be expressed as

$$MF_{G\rightarrow T}^{+ER} = [M^{lb}]/[WT^b + M^b + M^{lb}] \quad (3)$$

By solving equation (1) for $[WT^b + M^b]$ and equation (2b) for M^{lb}, and substituting these quantities into equation (3), $MF_{G\rightarrow T}^{+ER}$ can be expressed in terms of the ratios, R_i and $R_{G\rightarrow T}$, which are experimentally determinable.

$$MF_{G\rightarrow T}^{+ER} = [R_{G\rightarrow T}]/[R_i + R_{G\rightarrow T}] \quad (4)$$

From the values in Table I,

$$MF_{G\rightarrow T}^{+ER} = 0.0018 = [57/358\,000]/[0.087 + (57/358\,000)]$$

$MF_{G\rightarrow T}^{-ER}$ which is the mutation frequency in excision repair deficient cells (i.e. AB1885), can be estimated according to

$$MF_{G\rightarrow T}^{-ER} = MF_{G\rightarrow T}^{+ER} \times R_i(\text{AB1157})/R_i(\text{AB1885}) \quad (5)$$

From the values in Table I,

$$MF_{G\rightarrow T}^{-ER} = 0.0087 = 0.0018 \times 0.087/0.018$$

The rationale for this calculation is given in the Discussion, but hinges on the notion that DNA repair increases the yield of wild-type progeny plasmids in going from Uvr$^-$ to Uvr$^+$ cells, but does not affect the probability that unrepaired (+)-*anti*-B[*a*]P-N^2-Gua adducts will be misreplicated to generate mutations.

$MF_{G\rightarrow T}^{-ER}$ was calculated similarly for C-pUC19 (−SOS) and C-pUC19 (+SOS), but these values are probably not sensible, given that the $G_{437} \rightarrow T$ mutations from C-pUC19 are not likely to be derived from an adduct.

Results

Construction of (+)-anti-B[a]P-N^2-Gua-pUC19

The major adduct derived from (+)-*anti*-BPDE involves *trans* addition to give (+)-*anti*-B[*a*]P-N^2-Gua (Figure 1). This adduct was inserted into the unique *Pst*I site of pUC19 to give a plasmid designated (+)-*anti*-B[*a*]P-N^2-Gua-pUC19 (Figure 2), using methods virtually identical to those used by us previously (40; Materials and methods). The following should be noted.

1. Figure 2(a) shows that the construction of (+)-*anti*-B[*a*]P-N^2-Gua-pUC19 hinges on the ligation of the oligonucleotide 5′-pT[B[*a*]P-N^2]GCA-3′ into a gapped duplex. The adduct in (+)-*anti*-B[*a*]P-N^2-Gua-pUC19 can either replace G_{437} in one strand (pathway A) or G_{438} (pathway B) in the complementary strand (Figure 2; step 6). These species are shown

more explicitly in Figure 2(c). G_{437} and G_{438} are encountered during leading strand and lagging strand DNA synthesis respectively.

2. UV damage was included in the DNA strand that did not include the (+)-*anti*-B[*a*]P-N^2-Gua adduct in order to minimize the problem of strand bias (4,5,53), which is discussed below. The UV damage is represented by the dashed lines in Figure 2.
3. The *Pst*I site in pUC19 is in a *lacZ'* gene, which permits α-complementation to give β-galactosidase activity in appropriate cells (54). β-galactosidase activity can be monitored by the inclusion of the gratuitous inducer IPTG and the substrate, X-gal, which when cleaved gives colonies a blue color.

Transformation with (+)-anti-B[a]P-N^2-Gua-pUC19

(+)-*anti*-B[*a*]P-N^2-Gua-pUC19 and C-pUC19, which is a control plasmid constructed identically but with no adduct, were transformed (Figure 2b; step 7) into *E.coli* AB1157 (*uvr*$^+$) and AB1885 (*uvrB5*) cells using electroporation (44), which appears not to induce SOS (L.N.Naser-Bradley and J.M.Essigmann, personal communication) or damage the adduct (Materials and methods). (At this stage, information dependent upon *lacZ'* α-complementation could not be obtained because AB1157 and AB1886 cells are Lac$^+$.) Ampicillin-resistant cells were grown overnight (Figure 2b; step 8) and plasmid DNA was isolated from these cells and served as the permanent record of the experiment (Figure 2b; step 9). This DNA is designated R0 DNA (for 'round 0') and represents a mixture of plasmids generated from pathways A−C in Figure 2.

Analysis of transformants from R0 DNA derived from (+)-anti-B[a]P-N^2-Gua-pUC19 and C-pUC19

DH5-alpha cells were transformed with R0 DNA and plated (Figure 2; steps 10 and 11). Figure 2(b) explicitly includes steps leading to the generation of mutant progeny plasmids from the bypass of (+)-*anti*-B[*a*]P-N^2-Gua, which is represented by pathways A and B. Unfortunately, progeny plasmids attributable to genetic engineering side reactions were also formed (Figure 2b; pathway C) as discussed below. In the case of Figure 2, the designation step 6A implies step 6 in pathway A, etc. (For convenience plasmids are represented as both ovals and circles.)

Colonies appeared either dark blue, white, light blue or faintly blue after step 11 in Figure 2. Each colony color contains slightly different progeny plasmids and Table II provides a key, while a thorough discussion of the nature and characterization of each is presented in Materials and methods.

The vast majority of the dark blue colonies derived from transformations with (+)-*anti*-B[*a*]P-N^2-Gua-pUC19 (or C-pUC19) contained no mutations at the genome location in pUC19 originally occupied by the adduct, i.e. they were *Pst*I$^+$ and wild-type. This was established by DNA sequencing and *Pst*I digestion (see below).

White colonies arose from cells containing a plasmid derived via a genetic engineering side reaction, which can be understood by following steps 5−11 in pathway C of Figure 2 (Materials and methods). It is important to note that plasmids following step 6C in Figure 2: (i) are missing four base pairs from the *Pst*I recognition site, which makes them *Pst*I$^-$, and which results in a *lacZ'* frameshift mutation that prevents α-complementation; and (ii) have neither a (+)-*anti*-B[*a*]P-N^2-Gua adduct nor UV damage in either strand, which is significant (see below). Frameshift mutants obtained by analogous steps have been observed in other site-directed studies (46−48) and actually have proven useful as internal standards in the calculation of mutation frequency.

Colonies that were faintly blue were shown to contain progeny plasmids with a 5 bp deletion, and were generated by a slight variation on pathway C in Figure 2 (Materials and methods). Pathway D (Figure 2) does not efficiently generate progeny plasmids following transformation because UV damage is located in both strands.

Table I gives the initial ratio, R_i, of blue to 'white' colonies following transformation of R0 DNA into both Uvr$^+$ and Uvr$^-$ cells (i.e. following steps 10 and 11 in Figure 2). (At this stage it is difficult to distinguish between white, faintly blue and light blue colonies; thus 'white' here merely means 'not dark blue'. Mathematically, this is expressed correctly in equation 1.)

During construction of C-pUC19, pathway C in Figure 2 also occurred and also ultimately generated colonies that appeared white. This pathway must be fairly significant because ~60% of the colonies were white based upon R_i for C-pUC19 (Table I). The reason for this is readily understandable. White colonies came from plasmids with no UV damage in either strand (Figure 2; pathway C). In contrast, C-pUC19 itself, which generates blue colonies via pathways A and B in Figure 2 (though there was no adduct in the oligonucleotide), had UV damage in one of its strands, which decreased its ability to generate progeny. In fact in two similar studies with M13mp19 vectors constructed virtually identically to C-pUC19 except that no UV damage was present (27; M.Benasutti and E.L.Loechler, unpublished data), the fraction of white colonies was <5%. While not a direct comparison, this suggests that the yield of blue colonies via pathways A and B is artificially low compared to the yield of white colonies via pathway C because the former has UV damage in one strand while the latter has UV damage in neither strand.

The blue/white ratio (Table I) for transformations with (+)-*anti*-B[*a*]P-N^2-Gua-pUC19 [R_i(AB1157) = 0.087; Table I] is ~7.8-fold lower than with C-pUC19 in AB1157 cells [R_i(AB1157) = 0.69; Table I]. Because the genetic engineering reaction that generates the white colonies (Figure 2; pathway C) was expected to occur identically in the construction of (+)-*anti*-B[*a*]P-N^2-Gua-pUC19 and C-pUC19, the ~7.8-fold difference is likely to reflect a difference in the yield of blue colonies. This is attributed to the fact that the ligation efficiency of adduct-containing oligonucleotide 5′-T[B[*a*]P-N^2]GCA-3′ into gapped duplexes to give (+)-*anti*-B[*a*]P-N^2-Gua-pUC19 was ~6-fold lower than for the ligation of unadducted 5′-TGCA-3′, to give C-pUC19 (steps 5A and 5B in Figure 2; Materials and methods). Several other studies using short adduct-containing oligonucleotides have also observed that the presence of an adduct decreased the ligation efficiency (46−48). (We note that steps were taken to ensure that no gapped duplexes that could generate wild-type progeny remained in the ligation mixture; Materials and methods.)

The fact that the blue/white ratio for (+)-*anti*-B[*a*]P-N^2-Gua-pUC19 decreased in going from AB1157 (*uvr*$^+$) cells to AB1885 (*uvrB5*) cells (Table I) demonstrated that wild-type progeny were generated from (+)-*anti*-B[*a*]P-N^2-Gua-pUC19 itself, and not from a contaminating plasmid with no adduct. The effect of SOS induction on progeny yield from (+)-*anti*-B[*a*]P-N^2-Gua-pUC19 is addressed in the Discussion.

Strand bias. In a situation where one DNA strand contains a lesion(s) from a bulky mutagen/carcinogen, while the complementary strand does not, progeny plasmids are preferentially derived from the strand with no lesion(s) (4,5,53). In order to minimize the generation of progeny plasmids from the strand not

containing the (+)-*anti*-B[*a*]P-N^2-Gua lesion, UV damage was introduced into it (Figure 2; step 4). A saturation dose of UV light was used and we estimate that >14 pyrimidine dimers and five [6–4] lesions were induced per DNA strand (43).

In spite of this, strand bias was not completely eliminated based upon the results with C-pUC19. The blue/white ratio (R_i) increased ~1.6-fold in going from AB1885 (Uvr^-) to AB1157 (Uvr^+) cells independent of SOS induction [i.e. comparing R_i(AB1885) versus R_i(AB1157) in Table I]. Blue colonies were derived from C-pUC19, which had UV damage in one strand (i.e. pathways A and B in Figure 2), while white colonies were derived from DNA containing no UV damage (i.e. pathway C in Figure 2). The simplest interpretation of these results is that in Uvr^+ cells ~40% (≈0.6/1.6 × 100%) of progeny from C-pUC19 were generated from the strand containing UV damage. (It is also possible that DNA repair of UV damage in one strand enhanced replication of the other strand.) While this value is higher than hoped, the consequences did not prevent us from isolating mutants from the adduct in (+)-*anti*-B[*a*]P-N^2-Gua-pUC19, and the situation was an improvement over not having damage in the strand not containing the adduct (4–6, 53).

Isolation of mutants from (+)-anti-B[a]P-N^2-Gua-pUC19 transformed into SOS induced AB1157 cells

R0 plasmid DNA (i.e. after step 9 in Figure 2) contained progeny DNA from a variety of sources, and included *Pst*I^+ (i.e. wild-type) progeny plasmids derived from replication bypass of (+)-*anti*-B[*a*]P-N^2-Gua. *Pst*I treatment of R0 DNA (Figure 3; step 1) gave a mixture (designated R1 DNA) in which *Pst*I^+ plasmids were cleaved and linearized, and therefore did not transform efficiently. Thus, following transformation of R1 plasmid DNA (Figure 3; step 2), only colonies containing mutant *Pst*I^- plasmids were found (Materials and methods).

Following this mutant enrichment procedure, the colonies from the (+)-*anti*-B[*a*]P-N^2-Gua-pUC19 (SOS-induced) sample were principally (>99%) white (Table I), and attributable to the genetic engineering side reaction depicted as pathway C in Figure 2.

All in-frame *Pst*I^- mutants were in principle detectable. For example, $G_{437} \rightarrow A$, $G_{437} \rightarrow C$, $G_{438} \rightarrow A$, $G_{438} \rightarrow T$ and $G_{438} \rightarrow C$ mutations are *Pst*I^- and would generate dark blue colonies. ($G_{437} \rightarrow T$ is a special case and is discussed in the next paragraph.) In all of our work, one single dark blue mutant was identified and its plasmid was shown by DNA sequencing to have a $G_{437} \rightarrow C$ mutation. This is one position originally occupied by the adduct (Figure 2c) and suggests that this mutation was indeed caused by (+)-*anti*-B[*a*]P-N^2-Gua.

A small fraction of the colonies appeared light blue and were isolated for analysis. Similarly all colonies that appeared even faintly blue were also isolated. Light blue colonies arose from a plasmid with a $G_{437} \rightarrow T$ mutation induced by (+)-*anti*-B[*a*]P-N^2-Gua during leading strand DNA synthesis. This mutation changed a $\overset{5'\text{-}TGC\text{-}3'}{3'\text{-}ACG\text{-}5'}$ codon (where $\underline{G}$ indicates the site of the adduct) into an in-frame opal stop codon (i.e. $\overset{5'\text{-}TGA\text{-}3'}{3'\text{-}ACT\text{-}5'}$), which gave light blue colonies when plated on an opal suppressor strain due to partial suppression (46,47). The light blue colonies (as well as faintly blue colonies) were collected (Figure 3; step 3a), regrown on a plate (Figure 3; step 4a) and subjected to colony hybridization using a 16 base oligonucleotide specific for the $G_{437} \rightarrow T$ mutation in the *Pst*I recognition site (Figure 3; step 5a). Figure 4(a) shows typical results where one out of 25 colonies gave a positive signal. Plasmids were isolated from positive colonies and the $G_{437} \rightarrow T$ change was confirmed by DNA sequencing (Figure 3; step 6a).

Initially plasmids from non-hybridizing colonies were also sequenced. In large part these proved to be 5 bp deletion mutations in the *Pst*I site. These were consistently faintly blue, and were attributed to a side-reaction in the genetic engineering protocol that is a slight modification of pathway C in Figure 2 (Materials and methods). Occasionally, 4 bp deletion mutants were also isolated by this procedure, which indicates that we were conservative in what we chose as a 'light blue' or 'faintly blue' colony. [We note that we had originally thought that having a phenotypic screen for the $G_{437} \rightarrow T$ mutations (i.e. their light blue colony color) would prove to be an advantage. However, the unexpected finding that 5 bp deletion mutants appeared faintly blue confounded the search for the $G_{437} \rightarrow T$ mutants.] After ~200 of the plasmids from non-hybridizing colonies were sequenced, we stopped sequencing every one, and merely spot-checked ~10% of them. A second method was used to corroborate that all $G_{437} \rightarrow T$ mutants had been isolated (i.e. method 2 of Figure 3; Materials and methods).

Mutants were collected three times for transformations of (+)-*anti*-B[*a*]P-N^2-Gua-pUC19 into SOS induced cells, and the fraction of $G_{437} \rightarrow T$ mutations was similar in each case. A total of 57 $G_{437} \rightarrow T$ mutations were identified out of ~358 000 colonies (see $R_{G \rightarrow T}$ in Table I). The composite results were used to calculate the mutation frequency, $MF^{+ER}_{G \rightarrow T} \approx 0.18\%$ (based upon equation 4; Materials and methods), where '+ER' refers to the transformation of cells that are excision repair proficient (i.e. AB1157 cells).

Isolation of mutants from (+)-anti-B[a]P-N^2-Gua-pUC19 transformed into SOS uninduced AB1157 cells

The procedures described above were also used to isolate mutations from the transformation of (+)-*anti*-B[*a*]P-N^2-Gua-pUC19 into non-SOS-induced cells. Only $G_{437} \rightarrow T$ mutations were detected. $MF^{+ER}_{G \rightarrow T} \approx 0.04\%$ was estimated (Table I).

Isolation of mutants from C-pUC19 transformed into both SOS-induced and uninduced cells

Finally, no mutants, including no $G_{437} \rightarrow T$ mutations ($< \sim 0.3 \times 10^{-5}$), were found from transformations of C-pUC19 into SOS-induced cells. In contrast, the $G_{437} \rightarrow T$ mutation was observed at a low frequency ($\sim 0.3 \times 10^{-5}$) from transformations of C-pUC19 into non-SOS-induced cells (Table I).

Discussion

$G_{437} \rightarrow T$ mutations came from (+)-anti-B[a]P-N^2-Gua adducts in (+)-anti-B[a]P-N^2-Gua-pUC19

We studied the mutations induced by (+)-*anti*-B[*a*]P-N^2-Gua in a *Pst*I sequence context using methods that would have permitted us to detect any base pairing mutation that might have been induced by the adduct located at either G_{437} or G_{438}. The overwhelmingly dominant mutation detected was a $G_{437} \rightarrow T$ transversion mutation, which appeared at a frequency of ~0.18% in Uvr^+, SOS-induced cells (Table I). Six arguments suggest that this mutation is indeed derived from (+)-*anti*-B[*a*]P-N^2-Gua, and that its frequency of appearance is reasonable.

1. The oligonucleotide containing (+)-*anti*-B[*a*]P-N^2-Gua (i.e. 5′-TG(B[*a*]P-N^2)CA-3′) was extensively purified and its purity established; no other adduct-containing oligonucleotides were detected at the <0.1% level (40). Thus, the likelihood that a contaminating adduct is responsible for the mutation is remote.
2. The $G_{437} \rightarrow T$ mutations were isolated at a frequency ~10^3

higher from transformations with (+)-*anti*-B[*a*]P-N^2-Gua-pUC19 than from C-pUC19 (Table I). Nevertheless, this mutation was observed with C-pUC19 in SOS-uninduced cells. The following points argue that the source of the $G_{437} \rightarrow T$ mutants in experiments with (+)-*anti*-B[*a*]P-N^2-Gua-pUC19 could not possibly be the presence of a small fraction of a contaminating plasmid in the starting material that contained the $G_{437} \rightarrow T$ mutation: (i) no such mutants were isolated when C-pUC19 was transformed into SOS-induced cells; (ii) the absolute number of $G_{437} \rightarrow T$ mutants isolated from (+)-*anti*-B[*a*]P-N^2-Gua-pUC19 was always much higher than from C-pUC19; and (iii) (+)-*anti*-B[*a*]P-N^2-Gua-pUC19 gave more mutants in SOS-induced cells. Finally, in a separate experiment, (+)-*anti*-B[*a*]P-N^2-Gua-pUC19 was constructed and transformed into SOS-induced AB1157 cells; 61 $G_{437} \rightarrow T$ mutants were isolated, and $MF_{G\rightarrow T}^{+ER} \approx 0.46\%$ (and $MF_{G\rightarrow T}^{-ER} \approx 1.8\%$ as explained below) were calculated. [We note that variation in the 2- to 3-fold range has been observed by others in similar studies with adducts constructed by site-directed means (48; L.N.Naser-Bradley and J.M.Essigmann, personal communication).] This result corroborates the data in Table I and supports the notion that the mutations are indeed derived from the (+)-*anti*-B[*a*]P-N^2-Gua adduct in (+)-*anti*-B[*a*]P-N^2-Gua-pUC19.

3. The mutation reported herein for (+)-*anti*-B[*a*]P-N^2-Gua, which is $G \rightarrow T$, is not unexpected for this adduct because this mutation dominates the mutational specificity of BPDE (27−35) and this is the major adduct of BPDE. In the final section of this paper, data are presented that reinforce this conclusion.
4. In a separate study, we have determined the mutations induced by the pure stereoisomers, (+)-*anti*-BPDE, in a *supF* gene using a plasmid-based system, which we have recently developed for *E.coli* (55). $G \rightarrow T$ mutations were obtained in SOS-induced, Uvr^+ cells at a frequency of ~0.02−0.2% per adduct depending upon the site. This is in the range observed for (+)-*anti*-B[*a*]P-N^2-Gua in this site-directed study.
5. The fraction of wild-type progeny generated from (+)-*anti*-B[*a*]P-N^2-Gua-pUC19 decreased ~5-fold in going from Uvr^+ to Uvr^- cells (Table I). If we assume that excision repair enhances the yield of wild-type progeny, but does not affect the probability that an unrepaired (+)-*anti*-B[*a*]P-N^2-Gua adduct will give a mutation—a reasonable assumption—then the mutation frequency per adduct in Uvr^- cells (i.e. $MF_{G\rightarrow T}^{-ER}$) is estimated to be ~1% (Table I). This value is in reasonable agreement with an estimate of MF ~3% per adduct derived from (±)-*anti*-BPDE in Uvr^- *Salmonella* cells (58). Obviously, we are interested in confirming this result experimentally; however, the results of others (6,59,60) suggest that SOS induction in Uvr^- cells may not always be straightforward, which may preclude a direct investigation. In fact, our method to estimate $MF_{G\rightarrow T}^{-ER}$ may prove to be preferable, at least for studies involving plasmids, because full SOS induction is possible in Uvr^+ cells and the assumption mentioned above is reasonable.
6. The mutation frequency per adduct has been estimated to be ~1−3% for a variety of bulky adducts, including *cis*-DDP(ApG) (5), AF-C8-Gua (6), AFB_1-*N*7-Gua (60) and *cis*-DDP(GpG) (L.N.Naser-Bradley and J.M.Essigmann, personal communication). Thus, a value of ~1% for (+)-*anti*-B[*a*]P-N^2-Gua seems reasonable since it is in the range observed for other bulky adducts.

Two concerns: no mutation from adducts at G_{438} and frameshift mutagenesis

We made the decision to use a short, adduct-containing oligonucleotide, because it provided better resolution of products during HPLC purification; in fact we established that our oligonucleotide was >99.9% pure (40). We also decided to use a plasmid-based, as opposed to a phage-based (or phagemid-based), vector so that replication had to occur via a process that closely mimics chromosomal leading/lagging strand DNA synthesis. The inevitable consequence of these two decisions was that (+)-*anti*-B[*a*]P-N^2-Gua-pUC19 was actually a mixture of two species with an adduct at either G_{437} or G_{438} (Figure 2c). This was not problematic in another study using a phage vector (46). However, this led to one confounding result: only mutations at G_{437} were obtained from (+)-*anti*-B[*a*]P-N^2-Gua adducts, in spite of the fact that (+)-*anti*-B[*a*]P-N^2-Gua-pUC19 was expected to be an equal mixture of plasmids with the adduct either at G_{437} or G_{438}. Several rationale for this observation are considered.

It is possible that ligation of the (+)-*anti*-B[*a*]P-N^2-Gua-containing oligonucleotide occurred unequally and, in fact, no (+)-*anti*-B[*a*]P-N^2-Gua adducts were located at G_{438}. While a formal possibility, this seems unlikely given both the symmetry of the ligation reaction (Figure 2), and that this kind of differential ligation has never been reported, especially in analogous cases (46).

Preferential repair of (+)-*anti*-B[*a*]P-N^2-Gua in the transcribed strand cannot be the explanation, because the $G_{437} \rightarrow T$ mutations must come from an adduct remaining in the transcribed strand.

A consideration of the models presented in Figure 5 suggests that preferential mutagenesis at G_{437} is reasonable given the nature of leading/lagging strand DNA replication and the presence of the UV lesions. A (+)-*anti*-B[*a*]P-N^2-Gua adduct at G_{437} is replicated during leading strand DNA synthesis (Figure 5a), in which case the UV lesions are not encountered prior to encountering the (+)-*anti*-B[*a*]P-N^2-Gua adduct. In contrast the adduct at G_{438} is replicated during lagging strand DNA synthesis (Figure 5b), which of course requires successful initiation of

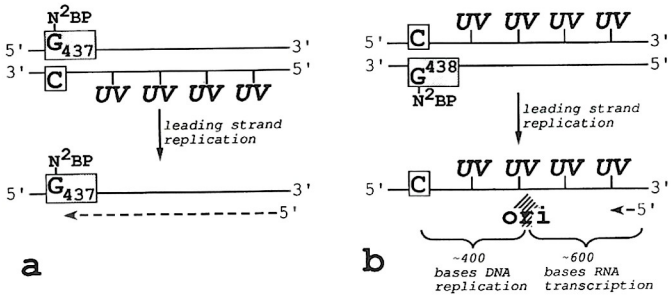

Fig. 5. Rationale for why $G_{437} \rightarrow T$, but not $G_{438} \rightarrow T$, mutations were detected in the study of mutagenesis by (+)-*anti*-B[*a*]P-N^2-Gua-pUC19. (**a**) Replication of the adduct at G_{437} occurred during leading strand DNA synthesis; there are no UV lesions in this strand. (**b**) Replication of the adduct at G_{438} occurred during lagging strand DNA replication, which can only occur following efficient initiation of leading strand DNA synthesis. Leading strand DNA synthesis requires the synthesis of an ~600 nucleotide RNA primer, which is processed by RNase H at the ColEI origin of replication (arrow) to provide a primer for the initiation of DNA synthesis (56,57), which must proceed ~400 nucleotides before the Cyt complementary to G_{438} is encountered. Both of these steps may be inhibited by the presence of the UV lesions in the strand being replicated during leading strand DNA synthesis.

leading strand synthesis. In the latter case, there are numerous UV lesions in the DNA strand that serves as the template during leading strand replication (Figure 5b). The ColEI origin in pUC19 is ~400 bp from G_{438} (54), so it seems reasonable to imagine that at least 400 nucleotides must be replicated on the leading strand before lagging strand synthesis of G_{438} can begin. UV lesions may also block leading strand replication if they block the synthesis of the RNA primer required to initiate leading strand DNA replication. This transcript is ~600 nucleotides in length and terminates at RNase H sites in the ColEI origin of pUC19 (56,57). Consequently, it seems reasonable to conclude that > ~40% of pUC19—in which there is expected to be > ~8 UV lesions prior to transformation—must either be transcribed or replicated during leading strand synthesis prior to the initiation of lagging strand synthesis that could ultimately result in the bypass of the (+)-*anti*-B[*a*]P-N^2-Gua adduct at G_{438}. Thus, it seems inevitable that the probability of the replication apparatus ever encountering G_{438} must be less than G_{437} and that the number of mutations from the former would be expected to be lower. (We note that if leading and lagging strand DNA synthesis are tightly coupled, then this inference might not be correct. However, the phenomenon of strand bias could not exist if leading and lagging strand DNA synthesis were absolutely coupled.) Furthermore, if it takes longer on average for the replication apparatus to encounter G_{438}, then there would also be more time for the adduct at G_{438} to be repaired (at least in Uvr^+ cells), which would also decrease the probability of mutagenesis at G_{438}.

Frameshift mutations induced by (+)-*anti*-B[*a*]P-N^2-Gua would generate white colonies. Unfortunately, the high frequency of white colonies derived from genetic engineering side reactions (i.e. pathway C in Figure 2) precluded an evaluation of frameshift mutagenesis in our study. However, other studies by us (55) and others (25) have suggested that BPDE induces frameshift mutations primarily in runs of G:C base pairs.

Effects of (+)-anti-B[a]P-N^2-Gua on genome survival

The ~5.1-fold decrease in progeny in going from Uvr^+ to Uvr^- cells (Table I) demonstrates that (+)-*anti*-B[*a*]P-N^2-Gua is repaired in Uvr^+ cells, and that the progeny yield from repaired vectors is higher than from non-repaired vectors, an obvious conclusion. This implies that (+)-*anti*-B[*a*]P-N^2-Gua blocks DNA replication and thereby contributes to lethality. C-pUC19 gave ~1.6-fold more wild-type progeny in Uvr^+ than Uvr^- cells (for reasons elaborated in Results), which implies that excision repair of the UV damage found in one strand of C-pUC19 can increase progeny yield. Thus, the ability of a single, site-specifically incorporated (+)-*anti*-B[*a*]P-N^2-Gua adduct to decrease progeny yield is estimated to be ~3.2 (= 5.1/1.6). If we assume that the majority—though clearly not all—of the (+)-*anti*-B[*a*]P-N^2-Gua adducts are repaired in Uvr^+ cells, then this single adduct appears to reduce replication efficiency to ~0.31 (i.e. 1/~3.2). This assumption is reasonable because the close correspondence between ligation yield and progeny yield (Results) would not have been observed if the majority of the (+)-*anti*-B[*a*]P-N^2-Gua adducts were not repaired in (+)-*anti*-B[*a*]P-N^2-Gua-pUC19.

SOS induction did not increase R_i(AB1157), which is the ratio of blue/white colonies, for (+)-*anti*-B[*a*]P-N^2-Gua-pUC19 in Uvr^+ cells (Table I), where an increase in R_i would have indicated an increase in blue, wild-type progeny derived from enhanced bypass of (+)-*anti*-B[*a*]P-N^2-Gua following SOS induction. This result is sensible because the majority of the (+)-*anti*-B[*a*]P-N^2-Gua adducts in (+)-*anti*-B[*a*]P-N^2-Gua-pUC19 were repaired as described in the previous paragraph. However, SOS induction also did not increase R_i for (+)-*anti*-B[*a*]P-N^2-Gua-pUC19 in Uvr^- cells (Table I). This could indicate either that SOS induction does not enhance survival for this adduct (at least as we have studied it), or that SOS induction does not occur efficiently in Uvr^- cells as discussed above. In this regard, we note that in our studies in *E.coli* with a plasmid randomly adducted with (+)-*anti*-BPDE, SOS induction did not appear to enhance the yield (i.e. survival) of progeny plasmids (55).

Role of (+)-anti-B[a]P-N^2-Gua adducts in mutagenesis by (+)-anti-BPDE

All detailed mutational studies with BPDE (27–35) have employed a mixture of the enantiomers (+)-*anti*-BPDE and (−)-*anti*-BPDE, which precludes a definitive comparison to our results for the pure (+)-*anti*-B[*a*]P-N^2-Gua adduct. However, GC → TA transversion mutations are the major mutation from (±)-*anti*-BPDE, which means that B[*a*]P-N^2-Gua adducts could in principle be responsible.

To evaluate this issue more definitively, we consider again our studies of the mutations induced by the pure stereoisomer, (+)-*anti*-BPDE, in a *supF* gene in *E.coli* (55). It is beyond the scope of this discussion to present the entire data set, but a comparison to the data for base pairing mutational specificity at G:C base pairs is germane. Overall, GC → TA mutations predominate (71% of the base pairing mutations at G:C base pairs), but GC → CG (18%) and GC → AT (11%) mutations are also found, which is comparable to what has been obtained with (±)-*anti*-BPDE (27–35). One striking result is that (to date) only GC → TA (i.e. 12/12; 100%) mutations have been detected when a Gua undergoing mutation is flanked on its 5′ side by a Thy (i.e. in 5′-T<u>G</u>-3′ sequences). This is in contrast to the situation in 5′-A<u>G</u>-3′, 5′-C<u>G</u>-3′ and 5′-G<u>G</u>-3′ sequences, where GC → TA mutations occur preferentially, but GC → CG and GC → AT mutations are also observed. This suggests that—by some mechanism—mutational specificity may be restricted by the presence of the Thy residue in a 5′-T<u>G</u>-3′ sequence.

Based upon the discussion in the previous paragraph, the results from our random mutagenesis studies with (+)-*anti*-BPDE in *supF* are consistent with the results presented herein, where G → T mutations were virtually exclusively isolated from a (+)-*anti*-B[*a*]P-N^2-Gua adduct studied site-specifically in a 5′-T<u>G</u>-3′ sequence. These results suggest that (+)-*anti*-B[*a*]P-N^2-Gua could be responsible for the mutations induced by (+)-*anti*-BPDE, at least in 5′-T<u>G</u>-3′ sequences.

The fact that a variety of bulky mutagens give mutation frequencies per adduct in the ~1–3% range, as observed here for (+)-*anti*-B[*a*]P-N^2-Gua, may be significant (5,6,61; L.N. Naser-Bradley and J.M.Essigmann, personal communication). First, it may imply that there are common elements to the pathway(s) by which these mutations are formed. Second, this suggests that > ~97% of the time these bulky adducts are not mutagenic. (This value is even higher in the absence of SOS induction.) It appears, therefore, that the adducts of bulky mutagens/carcinogens, e.g. (+)-*anti*-B[*a*]P-N^2-Gua, which do not disrupt the hydrogen-bonding face of the base moiety (Figure 1), are principally read without error by DNA polymerases *in vivo*. This is a remarkable result from which we can infer that DNA polymerases can be flexible without completely compromising fidelity.

Acknowledgements

We gratefully acknowledge the Cancer Research Program of the National Institutes, Division of Cancer Cause and Prevention, Bethesda, MD, for providing (+)-*anti*-BPDE. We thank Dr J.M.Essigmann for his comments on this manuscript, and him and Dr L.N.Naser-Bradley for communicating to us unpublished data. We thank Dr Gary Pauly for helpful discussions, especially regarding the rationale presented in Figure 5. This work was supported by NIH grant ES03775 and ACS grant CN-54.

References

1. Balmain,A. and Brown,K. (1988) Oncogene activation in chemical carcinogenesis. *Adv. Cancer Res.*, **51**, 147–182.
2. Miller,J.H. (1983) Mutational specificity in bacteria. *Annu. Rev. Genet.*, **17**, 215–238.
3. Basu,A.K. and Essigmann,J.M. (1988) Site-specifically modified oligonucleotides as probes for the structural and biological effects of DNA-damaging agents. *Chem. Res. Toxicol.*, **1**, 1–18.
4. Burnouf,D., Koehl,P. and Fuchs,R.P.P. (1989) Single adduct mutagenesis: strong effect of the position of a single acetylaminofluorene adduct within a mutation hot spot. *Proc. Natl. Acad. Sci. USA*, **86**, 4147–4151.
5. Burnhouf,D., Gauthier,C., Chottard,J.C. and Fuchs,R.P.P. (1990) Single d(ApG)*cis*-diamminedichloroplatinum (II) adduct-induced mutagenesis in *Escherichia coli*. *Proc. Natl. Acad. Sci. USA*, **87**, 6087–6091.
6. Reid,T.M., Lee,M.-S. and King,C.M. (1990) Mutagenesis by site-specific arylamine adducts in plasmid DNA: enhancing replication of the adducted strand alters mutation frequency. *Biochemistry*, **29**, 6153–6161.
7. Moriya,M., Takeshita,M., Johnson,F., Peden,K., Will,S. and Grollman,A.P. (1988) Targeted mutations induced by a single acetylaminofluorene DNA adduct in mammalian cells and bacteria. *Proc. Natl. Acad. Sci. USA*, **85**, 1586–1589.
8. Conney,A.H. (1982) Induction of microsomal enzymes by foreign chemicals and carcinogens by polycyclic aromatic hydrocarbons: G.H.A.Clowes memorial lecture. *Cancer Res.*, **42**, 4875–4917.
9. Phillips,D.H. (1983) Fifty years of benzo[*a*]pyrene. *Nature*, **303**, 468–472.
10. Phillips,D.H., Hewer,A. and Grover,P.L. (1985) Aberrant activation of benzo[*a*]pyrene in cultured rat mammary cells *in vitro* and following direct application to rat mammary glands *in vivo*. *Cancer Res.*, **45**, 4167–4174.
11. Marnett,L.J. (1987) Peroxyl free radicals: potential mediators of tumor initiation and promotion. *Carcinogenesis*, **8**, 1365–1373.
12. Cavalieri,E.L., Rogan,E.G., Devanesan,P.D., Cremonesi,P., Cerny,R.L., Gross,M.L. and Bodell,W.J. (1990) Binding of benzo[*a*]pyrene to DNA by cytochrome P-450 catalyzed one-electron oxidation in rat liver microsomes and nuclei. *Biochemistry*, **29**, 4820–4827.
13. Jeffrey,A.M., Jennette,K.W., Blobstein,S.H., Weinstein,I.B., Beland,F.A., Harvey,R.G., Kasai,H., Miura,I. and Nakanishi,K. (1976) Benzo[*a*]pyrene-nucleic acid derivative found *in vivo*: structure of a benzo[*a*]pyrenetetrahydrodiol epoxide-guanosine adduct. *J. Am. Chem. Soc.*, **98**, 5714–5715.
14. Koreeda,M., Moore,P.D., Yagi,H., Yeh,H.J.C. and Jerina,D.M. (1976) Alkylation of polyguanylic acid at the 2-amino group and phosphate by the potent mutagen (±)-7β,8α-dihydroxy-9β,10β-epoxy-7,8,9,10-tetrahydrobenzo[*a*]pyrene. *J. Am. Chem. Soc.*, **98**, 6720–6722.
15. Osborn,M.R., Beland,F.A., Harvey,R.G. and Brookes,P. (1976) The reaction of (±)-7β,8α-dihydroxy-9β,10β-epoxy-7,8,9,10-tetrahydrobenzo[*a*]pyrene with DNA. *Int. J. Cancer*, **18**, 362–368.
16. Jeffrey,A.M., Grzeskowiak,K., Weinstein,I.B., Nakanishi,K., Roller,P. and Harvey,R.G.(1979) Benzo[*a*]pyrene-7,8-dihydrodiol 9,10-epoxide adenosine and deoxyadenosine adducts: structure and stereochemistry. *Science*, **206**, 1309–1311.
17. Osborne,M.E., Harvey,R.G. and Brookes,P. (1978) The reaction of *trans*-7,8-dihydroxy-*anti*-9,10-epoxy-7,8,9,10-tetrahyroxybenzo[*a*]pyrene with DNA involves attack at the *N*7 position of guanine moieties. *Chem.-Biol. Interactions*, **20**, 123–130.
18. King,H.W.S., Osborne,M.E. and Brookes,P. (1979) The *in vitro* and *in vivo* reaction at the *N*7-position of guanine of the ultimate carcinogen derived from benzo[*a*]pyrene. *Chem.-Biol. Interactions*, **24**, 345–353.
19. Sage,E. and Haseltine,W.A. (1984) High ratio of alkali-sensitive lesions to total DNA modification induced by benzo[*a*]pyrene diol epoxide. *J. Biol. Chem.*, **259**, 11098–11012.
20. Rill,R.L. and Marsch,G.A.(1990) Sequence preferences of covalent DNA binding by *anti*-(+) and *anti*-(−)-benzo[*a*]pyrene diol epoxides. *Biochemistry*, **29**, 6050–6058.
21. Wen-Tah,H., Lin,E.J.S., Harvey,R.G. and Weiss,S.B. (1977) Mechanism of phage φX174 DNA inactivation by benzo[*a*]pyrene-7,8-dihydrodiol-9,10-epoxide. *Proc. Natl. Acad. Sci. USA*, **74**, 3335–3339.
22. Wang,Y., Maher,V.M., Liskay,R.M. and McCormick,J.J. (1988) Carcinogens can induce homologous recombination between duplicated chromosomal sequences in mouse L cells. *Mol. Cell. Biol.*, **8**, 196–202.
23. Kokontis,J.M., Vaughan,J., Harvey,R.G. and Weiss,S.B. (1988) Illegitimate recombination induced by benzo[*a*]pyrene diol epoxide in *Escherichia coli*. *Proc. Natl. Acad. Sci. USA*, **85**, 1043–1046.
24. McCann,J., Spingard,N.E., Kobori,J. and Ames,B.N. (1975) Detection of carcinogens as mutagens: bacterial tester strains with R factor plasmids. *Proc. Natl. Acad. Sci. USA*, **72**, 979–983.
25. Mizusaw,H., Lee,C.-H., Kakefuda,T., McKenney,K., Shimatake,H. and Rosenberg,M. (1981) Base insertion and deletion mutations induced in an *Escherichia coli* plasmid by benzo[*a*]pyrene-7,8-dihydrodiol-9,10-epoxide. *Proc. Natl. Acad. Sci. USA*, **78**, 6817–6820.
26. Wei,S.-J.C., Desai,S.M., Harvey,R.G. and Weiss,S.B. (1984) Use of short DNA oligonucleotides for determination of DNA sequence modifications induced by benzo[*a*]pyrene diol epoxide. *Proc. Natl. Acad. Sci. USA*, **81**, 5936–5940.
27. Eisenstadt,E., Warren,A.J., Porter,J., Atkins,D. and Miller,J.H. (1982) Carcinogenic epoxides of benzo[*a*]pyrene and cyclopenta[*cd*]pyrene induce base substitutions via specific transversions. *Proc. Natl. Acad. Sci. USA*, **82**, 1945–1949.
28. Bernelot-Moens,C., Glickman,B.W. and Gordon,A.J.E. (1990) Induction of specific frameshift and base substitution events by benzo[*a*]pyrene diol epoxide in excision-repair-deficient *Escherichia coli*. *Carcinogenesis*, **11**, 781–785.
29. Levin,D.E. and Ames,B.A. (1986) Classifying mutagens as to their specificity in causing the six possible transitions and transversions: a simple analysis using the *Salmonella* mutagenicity assay. *Environ. Mutagenesis*, **8**, 9–28.
30. Yang,J.L., Maher,V.M. and McCormick,J.J. (1987) Kinds of mutations formed when a human shuttle vector containing adducts of (±)-7β,8α-dihydroxy-9α,10α-epoxy-7,8,9,10-dihydrobenzo[*a*]pyrene replicates in human cells. *Proc. Natl. Acad. Sci. USA*, **84**, 3787–3791.
31. Carothers,A.M. and Grunberger,D. (1990) DNA base changes in benzo[*a*]pyrene diol epoxide-induced dihydrofolate reductase mutants of Chinese hamster ovary cells. *Carcinogenesis*, **11**, 189–192.
32. Mazur,M. and Glickman,B.W. (1988) Sequence specificity of mutations induced by benzo[*a*]pyrene-7,8-diol-9,10-epoxide at endogenous *aprt* gene in CHO cells. *Somat. Cell Mol. Genet.*, **14**, 393–400.
33. Chen,R.-H., Maher,V.M. and McCormick,J.J. (1990) Effects of excision repair by diploid human fibroblasts on the kinds and locations of mutations induced by (±)-7β,8α-dihydroxy-9α,10α-epoxy-7,8,9,10-dihydrobenzo[*a*]pyrene in the coding region of the *HPRT* gene. *Proc. Natl. Acad. Sci. USA*, **87**, 8680–8684.
34. Yang,J.-L., Chen,R.-H., Maher,V.M. and McCormick,J.J. (1990) Kinds and locations of mutations induced by (±)-7β,8α-dihydroxy-9α,10α-epoxy-7,8,9,10-dihydrobenzo[*a*]pyrene in the coding region of the hypoxanthine (guanine) phosphoribosyltransferase gene in diploid human fibroblasts. *Carcinogenesis*, **12**, 71–75.
35. Chen,R.-H., Maher,V.M. and McCormick,J.J. (1991) Lack of a cell cycle-dependent strand bias for mutation induced in the *HPRT* gene by (±)-7β,8α-dihydroxy-9α,10α-epoxy-7,8,9,10-dihydrobenzo[*a*]pyrene in excision repair-deficient human cells. *Cancer Res.*, **51**, 2587–2592.
36. Vousden,K.H., Bos,J.L., Marshall,C.J. and Phillips,D.H. (1986) Mutations activating human c-Ha-*ras1* protooncogene (*HRAS1*) induced by chemical carcinogens and depurination. *Proc. Natl. Acad. Sci. USA*, **83**, 1222–1226.
37. Bizub,D., Wood,A.W. and Skala,A.M. (1986) Mutagenesis of the Ha-*ras* oncogene in mouse skin tumors induced by polycyclic aromatic hydrocarbons. *Proc. Natl. Acad. Sci. USA*, **83**, 6048–6052.
38. Quintanilla,M., Brown,K., Ransden,M. and Balmain,A. (1986) Carcinogen-specific mutation and amplification of Ha-*ras* during mouse skin carcinogenesis. *Nature*, **322**, 78–83.
39. Pelling,J.C., Fischer,S.M., Neades,R., Strawhecker,J. and Schweickert,L. (1987) Elevated expression and point mutation of the Ha-*ras* protooncogene in mouse skin tumors promoted by benzoyl peroxide and other promoting agents. *Carcinogenesis*, **8**, 1481–1484.
40. Benasutti,M., Ezzedine,Z.D. and Loechler,E.L. (1988) Construction of an *Escherichia coli* vector containing the major DNA adduct of activated benzo[*a*]pyrene at a defined site. *Chem. Res. Toxicol.*, **1**, 160–168.
41. Howard-Flanders,P., Theriot,L. and Stedford,J.B. (1966) Three loci in *Escherichia coli* K-12 that control the excision of pyrimidine dimers and certain other mutagen products from DNA. *Genetics*, **53**, 1119–1136.
42. Hanahan,D. (1983) Studies on transformation of *Escherichia coli* with plasmids. *J. Mol. Biol.*, **166**, 557–580.
43. Brash,D.E. and Haseltine,W.A. (1982) UV-induced mutation hotspots occur at DNA damage hotspots. *Nature*, **298**, 189–192.
44. Dower,W.J., Miller,J.F. and Ragsdale,C.W. (1988) High efficiency transformation of *E.coli* by high voltage electroporation. *Nucleic Acids Res.*, **16**, 6127–6145.
45. Koffel-Schwartz,N., Verdier,J.M., Bichara,M., Freund,A.M., Daune,M.P. and Fuchs,R.P.P. (1983) Carcinogen-induced mutation spectrum in wild-type,

uvrA and *umuC* strains of *Escherichia coli. J. Mol. Biol.*, **177**, 35–51.
46. Loechler,E.L., Green,C.L. and Essigmann,J.M. (1984) *In vivo* mutagenesis by O^6-methylguanine built into a unique site in a viral genome. *Proc. Natl. Acad. Sci. USA*, **81**, 6271–6275.
47. Lasko,D.D., Harvey,S.C., Malaikal,S.B., Kadlubar,F.F. and Essigmann,J.M. (1988) Specificity of mutagenesis by 4-aminobiphenyl. *J. Biol. Chem.*, **263**, 15429–15435.
48. Basu,A.K., Loechler,E.L., Leadon,S.A. and Essigmann,J.M. (1989) Genetic effects of thymine glycol: site-specific mutagenesis and molecular modeling studies. *Proc. Natl. Acad. Sci. USA*, **86**, 7677–7681.
49. Parker,J. (1989) Errors and alternatives in reading the universal genetic code. *Microbiol. Rev.*, **53**, 273–295.
50. Atkins,J.F., Weiss,R.B. and Gesteland,R.F. (1990) Ribosome gymnastics—degree of difficulty 9.5, style 10.0. *Cell*, **62**, 413–423.
51. Ausubel,F.M., Brent,R., Kingston,R.E., Moore,D.D., Seidman,J.G., Smith,J.A and Struhl,K. (eds) (1989) *Short Protocols in Molecular Biology*. John Wiley, New York, pp. 185–194.
52. Sambrook,J., Fritsch,E.F. and Maniatis,E. (1989) *Molecular Cloning: A Laboratory Manual*. Cold Spring Harbor Laboratory Press, Cold Spring Harbor, NY. 2nd edn, Chapter 13, pp. 70–75.
53. Koffel-Schwartz,N., Maenhaut-Michel,G. and Fuchs,R.P.P. (1987) Specific strand loss in *N*-2-acetylaminofluorene-modified DNA. *J. Mol. Biol.*, **193**, 651–659.
54. Yanisch-Perron,C., Vieira,J. and Messing,J. (1985) Improved M13 phage cloning vectors and host strains: nucleotide sequences of M13mp19 and pUC19 vectors. *Gene*, **33**, 103–119.
55. Rodriguez,H., Drouin,E., Snow,E.T. and Loechler,E.L. (1992) Studies on mutations induced by the adducts of the (+)-*anti*-7,8-diol-9,10-oxide of benzo[*a*]pyrene (BPDE). *Proc. Am. Assoc. Cancer Res.*, **33**, 175 (abstract).
56. Tomizawa,J.I., Itoh,T., Selzer,G. and Som,T. (1981) Inhibition of ColEI RNA primer formation by a plasmid-specific small RNA. *Proc. Natl. Acad. Sci. USA*, **78**, 1421–1425.
57. Masukata,H. and Tomizawa,J.I. (1986) Control of primer formation for ColEI plasmid replication: conformational change for the primer transcript. *Cell*, **44**, 125–136.
58. Fahl,W.E., Scarpelli,D.G. and Gill,K. (1981) Relationship between benzo[*a*]pyrene-induced DNA base modification and frequency of reverse mutations in mutant strains of *Salmonella typhimurium*. *Cancer Res.*, **41**, 3400–3406.
59. Witkin,E.M. (1976) Ultraviolet mutagenesis and inducible DNA repair in *Escherichia coli*. *Bacteriol. Rev.*, **40**, 869–907.
60. Brouwer,J., van de Putte,P., Fichtinger-Schepman,A.M.J. and Reedijk,J. (1981) Base-pair substitution hotspots in GAG and GCG nucleotide sequences in *Escherichia coli* K-12 induced by *cis*-diamminedichloroplatinum(II). *Proc. Natl. Acad. Sci. USA*, **78**, 7010–7014.
61. Stark,A.A., Essigmann,J.M., Demain,A.L., Skopek,T.R. and Wogan,G.N. (1979) Aflatoxin B_1 mutagenesis, DNA binding, and adduct formation in *Salmonella typhimurium*. *Proc. Natl. Acad. Sci. USA*, **76**, 1343–1347.

Received on December 23, 1991; revised on March 16, 1992; accepted on March 19, 1992